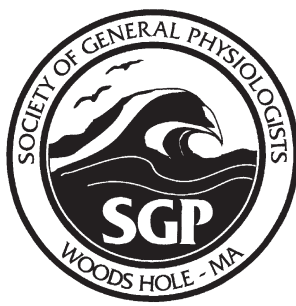


ABSTRACTS OF PAPERS AT THE SIXTY-FOURTH
ANNUAL MEETING OF THE SOCIETY
OF GENERAL PHYSIOLOGISTS

New optical methods in cell physiology

Marine Biological Laboratory
Woods Hole, Massachusetts
8–12 September 2010

Organized by
GRAHAM ELLIS-DAVIES



1. Laser-Scanning Intersecting Plane Tomography for High Speed, Translationless 3-D Microscopy. MATTHEW B. BOUCHARD and ELIZABETH M.C. HILLMAN, *Laboratory for Functional Optical Imaging, Department of Biomedical Engineering, Columbia University, New York, NY 10027*

Well-established imaging techniques, such as confocal or multiphoton microscopy, can provide exquisite three-dimensional (3D) images of biological tissues using absorption and fluorescence contrast. However, they acquire data via illumination point scanning, which provides limited 3-D scan rates, increased rates of photobleaching and photodamage, and an inability to perform real-time volumetric imaging of samples *in vivo*. Several new volumetric optical imaging techniques have been developed to overcome these limitations. Selective plane illumination microscopy (SPIM), ultramicroscopy, objective-coupled planar illumination microscopy, and oblique plane microscopy utilize the concept of light sheet imaging to image fluorescence contrast and can provide diffraction-limited resolution across 3-D volumes (Dodd, H.U., U. Leischner, A. Schierloh, N. Jährling, C.P. Mauch, K. Deininger, J.M. Deussing, M. Eder, W. Ziegler, K. Becker. 2007. *Nat. Meth.* 4:331–336; Dunsby, C. 2008. *Opt. Exp.* 16:20306–20316; Holekamp, T.F., D. Turaga, and T.E. Holy. 2008. *Neuron*. 57:661–672; Huisken, J., and D.Y. Stainier. 2009. *Development*. 136:1963–1975). Optical projection tomography (OPT) is a visible light analogue to x-ray computed tomography (CT), which acquires projection images and uses a modified back-projection algorithm to generate 3-D images of absorbing and/or fluorescent contrast (Sharpe, J., U. Ahlgren, P. Perry, B. Hill, A. Ross, J. Hecksher-Sørensen, R. Baldo, and D. Davidson. 2002. *Science*. 296:541–545). OPT and SPIM-type imaging techniques are limited to minimally or nonscattering samples, or larger *ex vivo*, chemically cleared samples. Additionally, the need for precise sample translation and/or rotation for OPT and SPIM significantly limits their volumetric scan rates. Here, we describe a new imaging technique: laser-scanning intersecting plane tomography (L-SIPT) (Bouchard, M.B., L. Grosberg, S.A. Burgess, and E.M. Hillman. 2010. *OSA Biomed.* BTuE7), which utilizes a non-contact imaging geometry similar to a confocal theta microscope and an off-axis detection geometry to provide high speed volumetric imaging of non- to minimally scattering tissues. The volume swept by L-SIPT can be scaled from micro- to macro-scales through the choice of an appropriate set of lenses. Here, we describe L-SIPT's imaging geometry and image reconstruction procedure, demonstrate how it can image microscale samples in 3-D and in real time, and show phantom results.

2. Two-Photon Microscopy of Neurovascular Dynamics *In Vivo*. BRENDA R. CHEN, ADDASON F.H. MCCASLIN, BARBARA L'HEUREUX, MATTHEW B. BOUCHARD, and ELIZABETH M.C. HILLMAN, *Laboratory for Functional Optical Imaging, Department of Biomedical Engineering, Columbia University, New York, NY 10027*

A regulated and localized change in blood flow dynamics accompanies almost all neuronal activity in the brain and is essential for normal brain function. Although this phenomenon, termed neurovascular coupling, forms the basis for commonly used functional brain imaging modalities such as fMRI, the mechanisms underlying the local hemodynamic response to brain activation remain poorly understood and widely debated. The lack of a cohesive model of neurovascular coupling is largely due to the difficulties associated with observing all of the different neuronal and vascular components involved, simultaneously *in vivo*.

To overcome this hurdle, we are using custom-designed optical imaging techniques, in conjunction with fluorescent dyes, to selectively visualize both vascular dynamics and the activity of major cell types in rodent cortex. Our high-speed multispectral two-photon microscopy system allows us to visualize the cellular activity, morphology, and interconnectivity of cortical neurons, astrocytes, pericytes, and interneurons, as well as blood flow and vasomotion in the vascular network. These can be imaged simultaneously using cell-specific fluorescent protein labeling, active dyes such as calcium-sensitive dyes, intrinsic fluorescence, and intravascular tracers. Supplementing these studies, our wider-field camera-based optical imaging system allows us to take high-speed multispectral images of cortical surface vessels with sufficient resolution to quantify changes in vessel diameters, blood flow, and blood oxygenation across the entire field of view. We are using both of these techniques to explore neurovascular coupling on multiple length scales in an effort to portray a complete picture of the cellular components and processes involved. We will present an overview of our imaging systems as well as our latest imaging results and a demonstration of the quantitative information that can be extracted from them.

3. An *In Vivo* Covalent TMP-Tag for Cell Imaging. SARAH S. GALLAGHER,¹ ZHIXING CHEN,¹ MICHAEL P. SHEETZ,² and VIRGINIA W. CORNISH,¹
¹*Department of Chemistry and ²Department of Biological Sciences, Columbia University, New York, NY 10027*

Chemical tags for live cell imaging are emerging as viable alternatives to the fluorescent proteins for labeling proteins with small molecule probes. Among reported chemical tags, trimethoprim (TMP)-tag stands out for having sufficient cell permeability and selectivity

to allow imaging of intracellular proteins. TMP-tag provides a noncovalent label in which the protein of interest is fused to *Escherichia coli* dihydrofolate reductase (DHFR) and then labeled with a cell-permeable TMP-probe heterodimer. To complement the utility of the noncovalent TMP-tag, we sought to render the TMP-tag covalent for applications such as single-molecule tracking and pulse-chase labeling that would benefit from a more permanent modification. On the basis of the long-standing use of proximity-induced reactivity for irreversible inhibitor design and its more recent application to *in vitro* chemical biology tools, we designed an eDHFR variant with a unique cysteine residue positioned to react with an acrylamide electrophile installed on the TMP-probe label. *In vitro* experiments show that the eDHFR:L28C nucleophile reacts rapidly and quantitatively with the TMP-acrylamide-probe. By tuning the distance between the TMP and the acrylamide, the time required for 50% alkylation of eDHFR:L28C was optimized to be 7 min. Most significantly, the balance in reactivity provided by the acrylamide electrophile allows intracellular proteins tagged with eDHFR:L28C to be labeled with a TMP-acrylamide-fluorescein heterotrimer in live cells with minimal background. Thus, proximity-induced reactivity is shown to be sufficiently selective for use in a living cell, suggesting a general approach for the development of orthogonal covalent chemical tags from existing noncovalent ligand–protein pairs. Moreover, the TMP electrophile described here can be used immediately as a covalent chemical tag in live cells, particularly in the field of *in vivo* cell imaging.

4. The Potential for Molecular Characterization of the Calcium-activated Potassium Channel in the Skate Electroreceptor. WILLIAM T. CLUSIN, *Cardiology Division, Stanford Medical Center, Stanford, CA, 94305*

Existence of distinct calcium-activated potassium channels was first proposed in 1974 based on voltage clamp experiments in the skate electroreceptor epithelium (Clusin, W.T., D.C. Spray, and M.V.L. Bennett. 1974. *Biol. Bull.* 147:472). The luminal surface of the electroreceptor epithelium (ampulla of Lorenzini) was shown to generate a potassium current that did not occur in the absence of calcium entry into the cells. The receptor cells are hair cells with a cilium on the luminal aspect and ribbon synapses on the basal aspect, which modulate the activity of afferent nerve fibers. Recent research has shown that calcium-activated potassium channels, called BK channels, are present at the apex of vertebrate hair cells and concentrated near the cilium. The BK channel has been cloned and sequenced in many species, and a partial sequence for *Raja erinacea* (617 bases) was recently published (GenBank accession no. FJ25726.1; Rohmann, K.N., D.L. Deitcher, and A.H. Bass. 2009. *Mol. Biol. Evol.* 26:1509–1521). This sequence includes the pore region and also S6.

BK channels are typically activated by both calcium and voltage. The calcium-activated potassium current in skate electroreceptor is unique because it cannot be activated by depolarization alone if calcium entry is blocked. This suggests a defect in the voltage sensor portion of the BK channel in skate electroreceptor, which could be due to a deletion or point mutation. The voltage sensor is normally on S4 of the BK channel. It is not certain if the BK channel nucleic acid sequence in the electroreceptor is identical to the sequence in whole brain, which was used to obtain the published sequence. Calcium-activated potassium channels are known to undergo alternative splicing, and it is possible that the channel in the electroreceptor contains a loss of function mutation in the voltage sensor region, which is not present elsewhere.

It is proposed that sequencing of messenger RNA from the skate electroreceptor epithelium could establish not only the presence of BK channels in the ampulla of Lorenzini, but also the reason for the apparent absence of activation by voltage.

5. Fluorescence Measurements to Examine the Conformational Dynamics of the Na,K-ATPase. ROBERT E.

DEMPSKI,¹ STEFAN GEYS,² and ERNST BAMBERG,²
¹*Department of Chemistry and Biochemistry, Worcester Polytechnic Institute, Worcester, MA 01609;* ²*Department of Biophysical Chemistry, Max Planck Institute of Biophysics, 60438 Frankfurt am Main, Germany*

The Na,K-ATPase is a critical protein for cellular homeostasis. It transports three sodium ions for two potassium ions across the plasma membrane and uses the energy from ATP hydrolysis to transport these cations against the concentration gradient. To correlate conformational changes with cation transport, we have combined fluorescence and electrophysiology methods to measure the conformational dynamics of the holoenzyme and to determine distance constraints between subunits of the enzyme. Furthermore, we have expanded these experiments to monitor conformational changes associated with electrogenic partial reactions of the Na,K-ATPase after changes in the concentration of internal sodium or external potassium. To probe the effects of the internal sodium concentration on the sodium branch of the Na,K-ATPase, oocytes were depleted of sodium and then loaded with sodium using the amiloride-sensitive epithelial sodium channel. The potassium branch of the Na,K-ATPase was studied by exposing the oocytes to different potassium concentrations in the presence and absence of internal sodium to obtain information on the apparent affinity for external potassium. Our results provide evidence on the relationship between lowering the internal concentration of sodium and increasing the amount of external potassium. Using fluorescence-based techniques, in combination with functional measurements, these experiments

demonstrate that it is possible to examine how external and internal ligands affect the conformational equilibrium of the ion pump on the surface of intact cells and have the potential to be expanded to a wide variety of membrane proteins.

6. Structural Rearrangements of the BK Channel Gating Ring Revealed by Patch Clamp Fluorometry. PABLO MIRANDA,¹ DIANA WESCH,¹ JORGE CONTRERAS,² MIGUEL HOLMGREN,² FRED SIGWORTH,³ and TERESA GIRALDEZ,¹ ¹*Unidad de Investigacion, Hospital Universitario Ntra Sra de Candelaria, 38010 Sta Cruz de Tenerife, Spain;* ²*NINDS/National Institutes of Health, Bethesda, MD 20892;* ³*Yale University School of Medicine, New Haven, CT 06510*

The large conductance voltage- and calcium-activated potassium channel (BK) is regulated by membrane voltage and intracellular calcium concentration. The calcium sensitivity of this channel is conferred by a large cytosolic domain. When calcium binds to this region, less energy is required to open the channel, but the exact mechanism underlying this process is not clear. The structure of MthK, a prokaryotic, calcium-activated potassium channel suggests that its intracellular calcium sensor domains (RCK) form a ring structure (the “gating ring”). Calcium binding could induce expansion of the gating ring, thus making the channel opening more energetically favorable by applying a force on the channel gate. Because BK cytosolic domain shares some homology with the calcium binding domain of MthK, it has been proposed that they function with similar calcium-sensing mechanisms. This idea is further supported by a BK structural model recently obtained by RSC cryo-EM (Wang, L., and F.J. Sigworth. 2009. *Nature*. 461:292–295). We have measured movements within the putative BK gating ring domain using FRET. BK heterotetramers containing both CFP- and YFP-tagged RCK domains have been formed. We have used patch clamp fluorometry to obtain fluorescence spectra of excised oocyte membrane patches expressing such heterotetramers with insertions in different sites along the gating ring region, including the linker between RCK1 and RCK2 domains, RCK2, the calcium bowl, and the rest of the C-terminal region. Depending on the site that is tagged, we detect changes in FRET due to changes in voltage or in calcium concentration. No changes are observed when the probe is inserted in the calcium bowl or the C-terminal region. These results are consistent with the model where a gating ring expands in response to increased calcium concentrations and suggest that only part of the C-terminal region forms this gating ring in BK.

7. Role of Intracellular Calcium Mobilization in Melanopsin-mediated Light Signalling in *Amphioxus*. JUAN MANUEL ANGUEYRA,¹ CAMILA PULIDO,²

GERARDO MALAGÓN,² ENRICO NASI,^{3,4} and MARÍA DEL PILAR GOMEZ,^{2,4} ¹*Department of Physiology and Biophysics, University of Washington, Seattle, WA 98105;* ²*Departamento de Biología and* ³*Instituto de Genética, Universidad Nacional de Colombia, Bogotá;* ⁴*Marine Biological Laboratory, Woods Hole, MA 02543*

The discovery of unconventional, nonvisual photoreceptors in the retina of mammals has challenged the dogma that lipid signaling for light transduction is a prerogative of microvillar cells of invertebrate eyes. Melanopsin, the photopigment of vertebrate “circadian” photoreceptors, is homologous to the rhodopsins of rhabdomeric photoreceptors, and mounting evidence indicates that it also signals through G_q and PLC. The nature of the downstream effectors, however, remains elusive. Pigmented ocelli and Joseph cells in the neural tube of *Amphioxus*, the most basal chordate, are microvilli-bearing primary photoreceptors that express melanopsin; because they are unambiguously identifiable and amenable to isolation and single-cell physiological assays, they provide a powerful model system to investigate melanopsin-mediated phototransduction mechanisms and their evolutionary history. We previously demonstrated in both cell types light-induced Ca mobilization from internal stores and dramatic attenuation of the photocurrent by intracellular Ca chelators. In the present study, pharmacological manipulations and whole cell patch clamp recording were used to assess the role of the IP₃ receptors. 2-APB and low molecular weight heparin were administered by local rapid superfusion and by intracellular dialysis, respectively, while cells were subjected to photostimulation. Both antagonists of the IP₃R caused a reduction of the photocurrent; however, the kinetics of activation remained extremely fast, manifesting none of the dramatic slow down that occurs in rhabdomeric photoreceptors. Concurrently, we failed to observe activation of a membrane conductance by administration of surrogates of diacylglycerol (DAG), such as the alkaloid (–) indolactam V or the phorbol ester PMA. The results are consistent with the notion that calcium released from the ER via IP₃-sensitive channels may fulfill a key role in conveying the light signal to the photoconductance, directly or indirectly, rather than serving as a modulatory side branch of the cascade that controls the kinetics of the enzymatic reactions.

Supported by National Science Foundation grant 0918930.

8. Molecular Identification of Two Isoforms of Arrestin in the Retina of Pecten: Role in Light Response Termination in Ciliary Invertebrate Photoreceptors. LADY ESPINOSA,¹ NELSON RAMIREZ,² MARÍA DEL PILAR GOMEZ,^{3,5} and ENRICO NASI,^{4,5} ¹*Graduate Program in Microbiology,* ²*Graduate Program in Neuroscience,* ³*Department of Biology, and* ⁴*Instituto de Genética, Universidad*

Nacional de Colombia;⁵ Marine Biological Laboratory, Woods Hole, MA 02543

The two canonical classes of visual receptors, rods, and cones and invertebrate microvillar photoreceptors diverge greatly in terms of downstream light-signaling mechanisms, but follow a similar general blueprint for the early steps of transduction and deactivation. Ciliary hyperpolarizing photoreceptors of mollusks have emerged as a third lineage in vision, with unique mechanisms of excitation and adaptation, but nothing was known about the turn-off of the activated photopigment. We used degenerate-primer PCR in *Pecten* retina cDNA to obtain two 600-bp amplicons highly homologous to arrestin, but differing in a stretch of 71 contiguous nucleotides. The diverging portion was exploited in nested RACE reactions to retrieve the full-length clones, and confirm that separate arrestin isoforms, dubbed Arr12 and Arr23, are expressed. The translated ORFs predict proteins with 425 and 416 amino acids, respectively, and molecular masses of 47 and 46 kD. The canonical N and C arrestin domains are present in both cases. Both isoforms are more homologous to β arrestins than visual arrestins, but lack the clathrin interaction motif in the carboxy tail, and are thus expected to quench metarhodopsin activity without promoting its endocytosis. The sequence identity of Arr12 and Arr23 is 81%, precluding differential localization in ciliary versus microvillar photoreceptors via *in situ* hybridization. Nonetheless, batteries of antibodies against vertebrate arrestins, previously screened in Western blots, show that for some of them, the immunoreactivity is confined to the distal retina, where ciliary photoreceptors are located. Intracellular dialysis and patch clamp recording indicate that anti-arrestin antibodies interfere with photocurrent shut-off and promote prolonged aftercurrents, even with chromatic stimulation designed not to cause the accumulation of large amounts of metarhodopsin. This novel lineage of light-sensing cells, therefore, uses canonical photopigment deactivation mechanisms, thus strengthening the case for a monophyletic evolutionary origin of visual mechanisms across metazoan.

Supported by National Science Foundation grant 0639774.

9. On the Transduction Gain of Melanopsin-mediated Light Signalling in *Amphioxus*: Single-Photon, Unitary, and Early Receptor Currents. MARÍA DEL PILAR GOMEZ^{1,3} and ENRICO NASI,^{2,3} ¹Departamento de Biología and ²Instituto de Genética, Universidad Nacional de Colombia, Bogotá; ³Marine Biological Laboratory, Woods Hole, MA 02543

Melanopsin, an ancient photopigment related to the rhodopsin of microvillar visual receptors in present-day invertebrates, has evolved in vertebrate organisms to subserve nonvisual light-sensing functions, like controlling the pupillary reflex and entraining the circadian rhythm. Compared to their counterparts in arthropods

and mollusks, circadian receptors in the vertebrate retina present no hint of a microvillar specialization and display an extremely reduced light sensitivity and uncommonly sluggish kinetics. Recently, bona fide melanopsin-expressing photoreceptors presumably ancestral to those of vertebrates have been characterized in the neural tube of *Amphioxus*, the most basal chordate. Known as Joseph and Hesse cells, they bridge the evolutionary gap between the photoreceptors of invertebrates and the circadian receptors of vertebrates. We used patch clamp recording to dissect the gain stage of the light transduction process. Dim illumination evoked distinct current fluctuations with a mean amplitude of 2–3 pA at -50 mV and a rapid time course (≈ 3 ms), attributable to melanopsin isomerizations produced by individual photons. Cell-attached recordings with stronger illumination revealed single-channel currents activated by light; the fast kinetics poses a challenge for accurate resolution, but the unitary amplitude is clearly in the 1-pA range, like those of invertebrate microvillar receptors. The gain can therefore be estimated to be substantially lower than in most rhabdomeric receptors, where 10^2 – 10^3 channels are recruited per photoisomerized rhodopsin. In contrast, high-speed measurements of responses to bright lights show fast transients, called early receptors currents (or ERCs), that precede the activation of the photoconductance and reflect the charge displacement upon the photo-induced conformational transition of melanopsin. The ERC density in *Amphioxus* is comparable to invertebrate rhabdomeric receptors; as a consequence, a reduction in the photopigment-to-channel coupling efficiency appears to be the primary cause underlying the low photosensitivity of melanopsin-utilizing light receptors in vertebrates.

Supported by National Science Foundation grant 0918930.

10. Characterization of Intrinsic Contrast in Intact Tissues Using Hyperspectral Two-Photon Microscopy. LAUREN E. GROSBERG, ANDREW J. RADOSEVICH, MATTHEW B. BOUCHARD, and ELIZABETH M.C. HILLMAN, *Laboratory for Functional Optical Imaging, Department of Biomedical Engineering and Department of Radiology, Columbia University, New York, NY 10027*

For most fluorescence microscopy techniques, contrast comes from exogenous dyes and autofluorescence must be minimized. However, removing intrinsic signals throws away valuable, readily available information about the chemical makeup of the specimen. Furthermore, exploiting intrinsic contrast allows repeatable imaging of a wide range of 3-D structures in intact fresh or even living tissue, without the need for histological processing, fixing, slicing, or staining.

Our hyperspectral two-photon microscopy technique allows detailed characterization of the two-photon excitation and emission spectrum of every voxel within a

sample. This approach is particularly valuable for intrinsic contrast imaging because it readily allows identification and segmentation of a wide range of tissue types, while also providing the possibility for quantitative analysis of the constituents of each tissue type (including NADH, FAD, elastin, collagen, keratin, etc.) (Radosovich, A.J., M.B. Bouchard, S.A. Burgess, B.R. Chen, and E.M. Hillman. 2008. *Opt. Lett.* 33:2164–2166).

We have used hyperspectral two-photon microscopy to image a range of murine tissues either *in vivo* or *perimortem*. These samples include tissue from the colon, small intestine, kidney, spleen, skin, and pancreas. We showed that in all of these tissues, intrinsic contrast revealed detailed 3-D morphology to depths of up to 500 microns without sectioning artifacts or the need for computational co-registration. Comparative histology of the same samples revealed good agreement between the structures visualized between the two techniques.

Beyond morphology, we are now validating the ability of hyperspectral two-photon microscopy to enable identification and quantification of specific intrinsic fluorophores. This will allow blind determination of tissue type, while also reporting the behavior of key endogenous fluorophores such as NADH and FAD in their native environment.

Our results suggest that hyperspectral two-photon microscopy could provide an alternative to conventional histology, particularly in settings where speed is important (such as during lesion excision or biopsy) or when there can be a benefit from visualizing key structures in 3-D. The method also has the potential for clinical translation for endoscopic applications.

11. Targeting Cyclic AMP Microdomains in Living Cells. KONSTANTINOS LEFKIMMIATIS, DANIELA LERONNI, SILVANA CURCI, and ALDEBARAN M. HOFER, *Department of Surgery, Harvard Medical School, VA Boston Healthcare System, and Brigham and Women's Hospital, West Roxbury, MA 02132; D. Leronni's present address is Dept. of Genetics and Microbiology, University of Bari, 70100 Bari, Italy*

The advent of FRET-based cAMP sensors has made possible the visualization of cAMP microdomains in living cells (Zaccolo, M., and T. Pozzan. 2002. *Science*. 295:1711–1715). However, the lack of available tools to perturb the cAMP microdomains *in situ* constitutes a major roadblock toward understanding the specific information potentially encoded by localized cAMP signals. Previously, we developed a genetically encoded mCherry-tagged cAMP buffer (cAMP sponge) (Lefkimiatis, K., M.P. Moyer, S. Curci, and A.M. Hofer. 2009. *PLoS ONE*. 4:e7649). This cytosolic construct was able to bind up cAMP and block the activation of its major effector, protein kinase A. Here, we propose that localized versions of our cAMP sponge can be used to selectively perturb cAMP microdomains, and we focus on the ex-

amples of the nuclear and mitochondrial compartments (Zippin, J.H., J. Farrell, D. Huron, M. Kamenetsky, K.C. Hess, D.A. Fischman, L.R. Levin, and J. Buck. 2004. *J. Cell. Biol.* 164:527–534; Acin-Perez, R., E. Salazar, M. Kamenetsky, J. Buck, L.R. Levin, and G. Manfredi. 2010. *Cell Metab.* 9:265–276). To achieve nuclear or mitochondrial targeting of our sponge, we used two tandem nuclear localization sequences and four mitochondrial localization signals, respectively. Confocal microscopy demonstrated that both constructs were highly expressed and efficiently localized in >90% of the transfected cells. To estimate the affinity and specificity of our targeted buffers, we performed pull down assays using agarose beads coated with a cAMP analog (Sp-2-AEA-cAMPS) as bait. Increasing doses of exogenous cAMP or high doses of cGMP were used to compete with Sp-2-AEA-cAMPS. Subsequent western blotting using specific antibodies showed that the nuclear and mitochondrial sponges bind cAMP specifically with roughly sub-micromolar affinity. Moreover, the introduction of point mutations in the cAMP binding domains rendered these constructs cAMP insensitive and provided an important negative control. Due to their high affinity, our targeted cAMP sponges promise to efficiently dampen local agonist-induced cAMP elevations, as well as putative constitutive signaling “micro-events,” unveiling the physiological roles of localized cAMP signals in resting and stimulated cells.

12. Benzodiazepines Modulate GABA-A Receptor Surface Levels and Synaptic Inhibition. T.C. JACOB,¹ G. MICHELS,² and S.J. MOSS,¹ ¹*Department of Neuroscience, Tufts University, Boston, MA 02111;* ²*Internal Medicine Clinic III, University of Cologne, 50937 Cologne, Germany*

Benzodiazepines potentiate the activity of gamma-aminobutyric acid receptors (GABA-ARs) and are widely used to treat anxiety, insomnia, and seizure disorders. However, the use of these therapeutic compounds is severely limited due to the development of tolerance. The molecular mechanism underlying benzodiazepine (BZ) tolerance is unknown. It is increasingly evident that BZ preferentially enhances the activity of synaptic GABA-AR subtypes that are largely composed of α 1-3, β 3, and γ 2 subunits. To directly address the role of BZ in regulating GABA-AR cell surface stability, we performed live imaging studies of pH-sensitive, GFP-tagged GABA-AR α 1(α 1-pHGFP) and α 2(α 2-pHGFP) subunits in hippocampal neurons to visualize the behavior of cell surface receptor populations. 24-hour treatment with the classical BZ flurazepam dramatically decreased α subunit cell surface levels. We measured total α 2 subunit levels by revealing pHGFP-tagged GABA-ARs inside the cell with NH4Cl. These live confocal studies showed that total neuronal α 2 subunit levels were lowered by BZs. These data suggest that BZs promote GABA-AR degradation, likely due to increased lysosomal degradation of

endocytosed receptors or increased endoplasmic reticulum-associated protein degradation via the proteasome. Next, we tested if the observed effect on BZ-sensitive GABA-AR surface levels is specifically induced by BZ binding. 1-hour treatment with the BZ antagonist flumazenil restored the BZ-lowered GABA-AR surface levels to control levels. The rapid time scale of flumazenil action is consistent with BZ-induced changes affecting receptor insertion and/or endocytosis rather than protein synthesis. Finally, we compared mIPSC properties in control neurons and those pretreated with flurazepam for 24 hours before recording. BZ treatment resulted in a decrease in mIPSC amplitude. Collectively, these data suggest that BZ treatment promotes the removal of α 2 subunit-containing GABA-ARs from the plasma membrane and their subsequent degradation, leading to a reduction in inhibitory synapse size and number, along with a decrease in the efficacy of synaptic inhibition.

13. Trimethoprim-based Chemical Tag for In Vivo Protein Labeling and Live Cell Imaging. CHAORAN JING, SARAH S. GALLAGHER, and VIRGINIA W. CORNISH, *Department of Chemistry, Columbia University, New York, NY 10027*

Over the past decade, chemical tags have emerged as viable tools to selectively label proteins in living cells. Combining the selectivity provided by genetic encoding and a modular small molecule fluorophore, chemical tags have been demonstrated to complement the utility of fluorescent proteins and facilitate demanding biophysical measurements in live cells. However, although it is now relatively straightforward to label cell surface proteins using chemical tags, developing a cell-permeable fluorescent probe with high signal-to-noise remains a challenging task. We previously demonstrated that the high-affinity interaction between *Escherichia coli* dihydrofolate reductase and trimethoprim (TMP) can be used to selectively label proteins with fluorescent tags inside living cells. Here, we present a TMP-based chemical tag with a modular organic fluorophore for two-photon live cell imaging. This TMP-fluorophore conjugate is shown to have appreciable two-photon excited fluorescence intensity and high cell permeability to allow efficient, high-resolution live cell imaging. We also present progress toward a TMP-based fluorogenic chemical tag aimed at enabling high signal-to-noise live cell super-resolution imaging. Collectively, our TMP-based chemical tags expand the tool kit available for labeling and visualizing intracellular proteins.

14. Altered Calcium Signaling in PMCA2^{+/−} Mice: Implications for Purkinje Cell and Cerebellar Function. AMANDA K. FAKIRA,^{1,2} LAWERENCE D. GASPERS,³ ANDREW P. THOMAS,³ and STELLA ELKABES,^{2,4}
¹*Integrative Neurosciences, UMDNJ-Graduate School of*

Biomedical Sciences, ²Department of Neurology and Neurosciences, ³Department of Pharmacology and Physiology, and ⁴Department of Neurosurgery and the Tim Reynolds Family Spine Research Laboratory, UMDNJ-New Jersey Medical School, Newark, NJ 07103

Plasma membrane Ca^{2+} ATPase isoform 2 (PMCA2), a pump required for Ca^{2+} extrusion from the cytosol, is most abundantly expressed in cerebellar Purkinje cells (PCs). We have previously reported that PMCA2 forms a complex with synaptic proteins and glutamate receptors mGluR1, GluR δ 2, and the AMPA receptor subunits GluR2/3. Fura-2 Ca^{2+} imaging on cultured PMCA2^{+/−} and PMCA2^{−/−} PCs was used to determine how PMCA2 may contribute to AMPA receptor signaling. Our results indicate that the amplitude of AMPA receptor-mediated Ca^{2+} transients are increased in PMCA2^{+/−} PCs compared with PMCA2^{+/+}. This is likely due to increased Ca^{2+} influx, as expression of P/Q-type voltage-gated Ca^{2+} channels (VGCC) is increased in PCs of the PMCA2^{+/−} mice in vitro. We also examined the expression of P/Q-type VGCC in PCs of the 3-week-old mouse cerebellum, as the maturity of the PCs at this age corresponds to that of PCs in vitro. In accordance, we found higher P/Q-type VGCC expression in 3-week-old PMCA2^{+/−} cerebella as compared with the PMCA2^{+/+}. In contrast, alterations in other mechanisms, such as sequestration into the endoplasmic reticulum or intracellular Ca^{2+} buffering, did not appear to contribute to higher amplitude.

In addition, we determined whether reduced PMCA2 expression affects the expression of glutamate receptors in the complex. We did not find any significant differences between PMCA2^{+/+} and PMCA2^{+/−} mice at 3 weeks. However, a significant decrease in GluR2/3 and mGluR1 levels was observed by 8 weeks of age. This was followed by a small but significant reduction in the number of PCs by 20 weeks of age. Thus, early abnormalities in Ca^{2+} influx and the subsequent aberrance in glutamate receptor expression could lead to delayed PC dysfunction and loss in the PMCA2^{+/−} mice.

15. Does a Specific Isoform of Adenylyl Cyclase Mediate Store-operated Cyclic AMP Signaling? ISABELLA MAIELLARO, KONSTANTINOS LEFKIMMIATIS, SILVANA CURCI, and ALDEBARAN M. HOFER, *Department of Surgery, Harvard Medical School, VA Boston Healthcare System, and Brigham and Women's Hospital, West Roxbury, MA 02132*

The various isoforms of adenylyl cyclase (AC1-AC9), the enzymes that generate cAMP, are differentially regulated and have been implicated in specific pathophysiological processes. For example, knocking down AC3 in mouse induces an obese phenotype (Wang, Z., V. Li, G.C. Chan, T. Phan, A.S. Nudelman, Z. Xia, and D.R. Storm. 2009. *PLoS One*. 4:e6979), whereas knockdown of AC5 prolongs lifespan and protects against stress

(Yan, L., D.E. Vatner, J.P. O'Connor, A. Ivessa, H. Ge, W. Chen, S. Hirotani, Y. Ishikawa, J. Sadoshima, and S.F. Vatner. 2007. *Cell*. 130:247–258). Our lab recently discovered a new pathway in which Ca^{2+} depletion from the endoplasmic reticulum (ER) causes cAMP to increase through activation of one or more isoforms of conventional AC in colonic epithelial cells. This “store-operated” process is independent of cytosolic $[\text{Ca}^{2+}]$ and requires the ER transmembrane protein, STIM1 (Lefkimiatis, K., M. Srikanthan, I. Maiellaro, M.P. Moyer, S. Curci, and A.M. Hofer. 2009. *Nat. Cell Biol*. 11:433–442). Here, we asked whether there is a unique AC isoform involved in store-operated cAMP production. Ca^{2+} stores were released using 5 μM ionomycin in a Ca^{2+} -free solution, resulting in a significant increase in cAMP, as measured using a FRET-based cAMP reporter in single colonic epithelial-derived cells. Transient overexpression of AC3 resulted in a statistically significant increase in cAMP production induced by ionomycin ($59.25 \pm 3.60\%$ of the maximal response; $n = 32$ cells), compared with control ($52.91 \pm 3.53\%$; $n = 32$; $P < 0.05$). In contrast, overexpression of AC5, AC6, or AC7 resulted in a statistically insignificant increase in cAMP production (AC5, $n = 13$ cells; AC6, $n = 12$ cells; AC7, $n = 15$ cells). Knockdown of AC3 using siRNA inhibited the ionomycin-induced elevation of cAMP ($41.40 \pm 2.28\%$; $n = 60$ cells; $P < 0.05$), whereas silencing of AC5 ($n = 68$ cells) or AC6 ($n = 91$ cells) had no effect. Thus far, our data indicate that AC3 may be specifically involved in cAMP production elicited by ER store depletion. This information may ultimately provide clues about the physiological function of store-operated cAMP signaling, and it may help to identify other components of this unusual signaling pathway.

16. Super-Resolution Imaging of Cardiac Signaling Microdomains by STED Microscopy. T. KOHL,¹ M.A. LAUTERBACH,² E. WAGNER,¹ V. WESTPHAL,² B. HAGEN,³ W.J. LEDERER,³ S.W. HELL,² and S.E. LEHNART,^{1,3} ¹*Heart Research Center Göttingen, Department of Cardiology and Pulmonology, University Medical Center, Göttingen, Germany*; ²*Department of Nanobiophotonics, Max Planck Institute for Biophysical Chemistry, 37077 Göttingen, Germany*; ³*Center for Biomedical Engineering and Technology, University of Maryland, Baltimore, MD 20742*

Structures for intracellular signaling in heart cells are compartmentalized within specialized microdomains, which are believed to be crucial for physiological function. However, these microdomains typically have dimensions that are below the resolution limit of conventional light microscopy; therefore, their structure and function are not well understood.

Methods. To overcome these limitations, we have examined two principal components of intracellular calcium release units (CRUs) by stimulated emission depletion (STED) microscopy: supramolecular clusters

of intracellular Ca^{2+} release channel/ryanodine receptors (RyR2s) and transverse tubules (TTs). Peripheral, immunolabeled CRUs near the plasma membrane of mouse cardiomyocytes were analyzed for RyR2 cluster size and structure. TTs were stained with the lipophilic dye di-8-ANEPPS in living cells to characterize their structure and diameters.

Results. Peripheral RyR2 clusters are often arranged in double rows centered on Z-lines. Within individual RyR2 clusters, by STED microscopy we readily identified substructures below the optical resolution limit of confocal imaging. RyR2 cluster shapes ranged from circular to asymmetric elongated. Clusters sometimes showed periodic substructures of yet unknown physiological relevance. RyR2 cluster sizes analyzed after image segmentation appear to show an exponential distribution. STED imaging in live cells resolved circular TT sections and TT network organization, while conventional confocal imaging could not resolve true TT structure. Accordingly, the average TT diameter (full width at half-maximum) determined by a 2-D Gaussian fit was in confocal images 262 ± 26 nm versus 233 ± 37 nm in STED images (mean \pm SD; $n = 391$; $P < 0.05$). Additionally, optical cross-sections of presumptive TTs showed a 1-peak intensity distribution in confocal images, whereas in STED images hollow structures could be resolved, consistent with morphometric identification of real tubular cross-sections.

Conclusions. STED microscopy optically resolves two major CRU domains in cells, RyR2 clusters, and TTs. This progress opens new windows to the study of complex signaling domains in heart cells and especially their dynamic reorganization in normal and diseased heart states.

17. Co-Stimulation through VLA-4 Inhibits Microcluster Movement by Resisting Myosin-dependent Contraction within the Synapse. ALENKA LOVY-WHEELER,¹ NICHOLAS R. SYLVAIN,² ROSEMARY R. BREWKA,² JON DEGNORE,³ and STEPHEN C. BUNNELL,⁴ ¹*Center for Neuroscience Research*, ²*Program in Immunology*, ³*Tufts Imaging Facility*, and ⁴*Department of Pathology, Tufts University School of Medicine, Boston, MA 02111*

Antigen receptors assemble signaling microclusters that contain the adapter SLP-76 and are transported toward the center of the immune synapse. These structures are essential for T cell activation; however, no clear rationale has been provided for their movement. Progress in this regard has been hindered by the obscurity of the mechanisms governing microcluster movement. Recently, we determined that the engagement of the a4b1 integrin (VLA-4) by immobilized counter-ligands greatly reduces the mobility of TCR-induced SLP-76 microclusters (SLP-MCs), and that this effect is associated with increased T cell activation. To test the hypothesis that microcluster immobilization promotes T cell activation

by enabling more sustained and more productive interactions between the TCR and SLP-MCs, we wished to identify and perturb the systems driving SLP-MC movement. Because our previous data suggested that SLP-MCs are intimately associated with adhesive structures and with the insoluble actin cytoskeleton, we developed a mechanical isolation procedure that allowed us to obtain highly purified TCR- and SLP-MCs, which were analyzed by LC/MS/MS. We find that myosin IIA is associated with SLP-MCs and plays a critical role in MC translocation. Rho kinase (ROCK)-activated myosin II is required to generate contractile, centralizing forces within the synapse; these forces are resisted after VLA-4 ligation, most likely through the engagement of a “molecular clutch” linking VLA-4 to the actin cytoskeleton. Importantly, SLP-MCs immobilized after the inactivation of myosin II do not contribute to T cell activation. Therefore, we propose that T cells are co-stimulated in response to the intracellular tension generated by the opposing activities of myosin II and VLA-4.

18. Optical Assays of Innate Immunity: *Pseudomonas aeruginosa* Homoserine Lactone Activates Store-operated cAMP and CFTR-dependent Cl⁻ Secretion by Human Airway Epithelia. S. WONG,¹ J. SHI,¹ E. MATTHES,¹ B. ILLEK,² J.P. IANOWSKI,³ R.J. ARANT,¹ E. ISACOFF,¹ H. VAIS,⁴ J.K. FOSKETT,⁴ I. MAIELLARO,⁵ A.M. HOFER,⁵ and T.E. MACHEN,¹ ¹Department of Molecular and Cell Biology, University of California, Berkeley, Berkeley, CA 94720; ²Children's Hospital Oakland Research Institute, Oakland, CA 94609; ³Department of Physiology, University of Saskatchewan, Saskatoon SK S7N 5E5, Canada; ⁴Department of Physiology, University of Pennsylvania Medical School, Philadelphia, PA 19104; ⁵Department of Surgery, Brigham and Women's Hospital, Harvard Medical School, West Roxbury, MA 02132

The bacterium *Pseudomonas aeruginosa*, bacteria that commonly infect the lungs of cystic fibrosis (CF) patients, secrete N-(3-oxo-dodecanoyl)-S-homoserine lactone (3O-C12) to regulate bacterial gene expression. 3O-C12 also affects functions of eukaryotic cells. Transsepithelial electrophysiology in Ussing chambers showed that 10–100 μM 3O-C12 increased Cl⁻ secretion (I_{Cl}) in CFTR-expressing airway epithelial cell lines, but not in CF cells. Bright field observations of “bubble” formation in oil-covered pig tracheas showed that 3O-C12 also increased fluid secretion by glands in non-CF pig trachea. Fura-2 imaging showed that 3O-C12 increased cytosolic [Ca²⁺]_c, Ca_{cyto}, similarly in Ca²⁺-containing and Ca²⁺-free solutions, indicating that Ca was being released from the endoplasmic reticulum. FRET imaging of camaleon D1-transfected cells confirmed that 3O-C12 reduced [Ca²⁺]_e in the endoplasmic reticulum (Ca_{ER}). The Ca²⁺-ATPase inhibitor thapsigargin (tg) also increased I_{Cl} and Ca_{cyto}, and decreased Ca_{ER}, and 3O-C12 had no effect in cells treated with tg. Patch clamp measure-

ments on isolated nuclei from IP₃R1-expressing DT40 cells showed that 3O-C12 also activated IP₃R1. TIRF imaging showed that 3O-C12 and tg both activated STIM1, an ER protein that regulates plasma membrane proteins. FRET imaging of Epac H30-transfected cells showed that 3O-C12 increased cytosolic [cAMP] (cAMP_{cyto}). 3O-C12-stimulated I_{Cl} was inhibited by a cAMP antagonist and increased by a phosphodiesterase inhibitor. The high K_d Ca²⁺ chelator TPEN, which lowers Ca_{ER} without increasing Ca_{cyto} in other cells, increased cAMP_{cyto} and I_{Cl}, similar to 3O-C12. It is concluded that 3O-C12 stimulates CFTR-dependent Cl⁻ and fluid secretion in airway epithelial cells by directly activating IP₃R, lowering Ca_{ER}, and activating STIM1 and store-operated cAMP production. In CF airways, 3O-C12 will alter Ca and cAMP signaling but will not increase Cl⁻ and fluid secretion.

19. Measurement of Cell Volume and Membrane Integrity in Adherent Cells. JENNIFER L. GREGG,¹ SAHIL M. PANDYA,² and MICHAEL A. MODEL,² ¹School of Biomedical Sciences and ²Department of Biological Sciences, Kent State University, Kent, OH 44023

Cell volume is one of the basic characteristics of a cell and is being extensively studied in relationship to diverse biological processes. At the same time, a simple microscopic technique for its measurement is lacking. The method we propose uses negative transmission contrast rendered to cells by a strongly absorbing dye present in the medium. Cells are placed in a perfusion chamber with a shallow (0.03-mm) channel, and a non-toxic dye, such as Acid Blue 9, is added to the medium. Transmission images are collected at the wavelength of maximum dye absorption (630 nm). Where the cells displace the dye, the thickness of the absorbing layer is reduced; thus, an increase in cell thickness produces brighter images, and vice versa. The results are unaffected by possible fluctuations in the light source, and a high S/N ratio can be achieved. Because cells in this method are only exposed to low-intensity light, the method is well suited for time-lapse experiments. To demonstrate the utility of this method, we investigated the volume response of T24 cells to a hypotonic buffer and to apoptosis-inducing chemicals staurosporine and ionomycin.

From the known absorption coefficient of the dye, the image contrast can be converted into the absolute values for cell thickness and volume. However, quantitative interpretation of the images relies on the assumption that the cell membrane is impermeable to the external dye. To test for possible membrane leakage caused by treatment with apoptotic agents, we labeled the cytoplasm with the red fluorescent probe CellTracker Orange. If the external dye penetrates the plasma membrane, it quenches CellTracker fluorescence, and from the extent of quenching the intracellular concentration of

Acid Blue 9 can be determined. In our experiments, partial loss of membrane integrity was indeed detected after treatment of cells with high concentrations of ionomycin.

20. Monitoring Protein Misfolding and Calcium Signaling during the Unfolded Protein Response (UPR). R. MADELAINE PAREDES,¹ and JAMES D. LECHLEITER,^{1,2} ¹*Department of Cellular and Structural Biology and ²Department of Physiology, University of Texas Health Science Center at San Antonio, San Antonio, TX 78229*

The endoplasmic reticulum (ER) is the main intracellular organelle for Ca^{2+} storage (Berridge, 2002). The ER is also the location where proteins destined to be secreted are synthesized, folded, and processed (Helenius, 1994; Parodi, 2000). It is well known that defects in the protein synthesis machinery or in the environment of the ER induce ER stress, which activates a mechanism called the unfolded protein response (UPR) that helps to restore ER homeostasis (Kaufman, 1999; Harding et al., 2002). If ER homeostasis cannot be restored by the UPR, a program of cell death is activated (Nakagawa et al., 2000; Scorrano et al., 2003; Hitomi et al., 2004; Li et al., 2006). In many conditions where protein misfolding occurs, there is a noticeable dysregulation in ER Ca^{2+} homeostasis (Haughey et al., 1999; Hetz et al., 2003; Benali-Furet et al., 2005; Tu et al., 2006). However, it has not been established whether ER Ca^{2+} dysregulation is a cause or a consequence of misfolding. Here, we have developed imaging techniques to monitor the impact of ER Ca^{2+} depletion on protein processing and the effect that protein misfolding may have on ER Ca^{2+} . For this purpose, we partially depleted the ER stores using thapsigargin (Tg) on *Xenopus* oocytes expressing a model secreted protein carboxypeptidase Y (CPY-wt) (Finger et al., 1993). A mutant form of CPY that is known to be retained within the ER (CPY_{G255R}) was used as a control (Finger et al., 1993; Mancini et al., 2003). Both the wild-type and mutant forms of CPY were labeled with variants of the green fluorescent protein to directly visualize their retention in the ER by confocal microscopy. We found that partial depletion of ER Ca^{2+} with either 50 or 100 nM Tg for 48 hours induced significant induction of the UPR, as monitored by the phosphorylation of eIF2 α (P-eIF2 α), and induced ER retention and accumulation of CPY-wt. Partial depletion had no effect on ER retention of the mutant CPY (CPY_{G255R}). We also tested whether an accumulation of misfolded proteins in the ER induced ER Ca^{2+} loss. We found that overexpression of the mutant misfolded protein (CPY_{G255R}) did not significantly affect ER Ca^{2+} levels (D1ER) or induce ER stress (P-eIF2 α) in *Xenopus* oocytes. However, inhibition of protein glycosylation by tunicamycin rapidly induced a Ca^{2+} leak from the ER within 5 minutes of treatment. In summary, partial Ca^{2+} depletion of the ER stores is sufficient to induce accu-

mulation of a normally secreted protein. Induction of significant protein misfolding also appears to induce ER Ca^{2+} loss. We suggest that Ca^{2+} may be both a cause and a consequence on the folding/misfolding process under the UPR.

21. Artificial Ca^{2+} Sparks in a Dual Confocal Scanner. A Rich Man's Stopped Flow for the Characterization of Ca^{2+} -reactive Molecules and Biosensors. LOURDES FIGUEROA,¹ JINGSONG ZHOU,¹ VYACHESLAV SHKRYL,¹ YAN LI,¹ JIANXUN YI,¹ ATSUYA MOMOTAKE,² LOTHAR BLATTER,¹ GRAHAM ELLIS-DAVIES,³ GUSTAVO BRUM,⁴ and EDUARDO RÍOS,¹ ¹*Rush University, Chicago, IL 60612; ²Tsukuba University, 305-8577 Ibaraki, Japan; ³Drexel University, Philadelphia, PA 19104; ⁴Universidad de la República, Montevideo, Uruguay*

Control of calcium signaling in striated muscle relies on concurrent actions of calcium ions to promote and inhibit release channel opening. As quantifiable local probes of these actions, we developed artificial Ca^{2+} sparks, which are generated by 2-photon (2P) release from various "cages." A "dual scanner" (510 LIVE Duo; Carl Zeiss, Inc.) delivers IR laser flashes to a diffraction-limited region through an LSM 510 scanner, while rapidly imaging fluorescence of a $[\text{Ca}^{2+}]$ monitor via a slit scanner (5-LIVE; \sim 100 μ s/line). Ca^{2+} sparks of 0.1–10 μM are elicited after microseconds of 2P irradiation at 720 nm and imaged with the low affinity dye fluo 4FF. Reaction-diffusion analysis (Ríos, E., M.D. Stern, A. González, G. Pizarro, and N. Shirokova. 1999. *J. Gen. Physiol.* 114:31–48) yields the flux of Ca^{2+} photorelease. This flux, which initially may reach several hundred mM/s, decays with τ of 2–3 ms when the cage is DM-nitrophen or 5–8 ms when the cage is the much more efficient NDBF-EGTA (Momotake, A., N. Lindegger, E. Niggli, R.J. Barsotti, and G.C. Ellis-Davies. 2006. *Nat. Methods.* 3:35–40). The kinetics of decay after the photolysing IR flash serves to quantify intrinsic photochemical properties of the cages. The technique was also used to quantify the response of the Ca^{2+} biosensors YC3.6 and D4, as well as the properties of calcium buffers used in intracellular solutions, including sulfate and glutamate. It is currently being explored as a tool to derive diffusion coefficients of sensors and buffers.

In sum, while the original goal was to use artificial sparks to quantitatively characterize calcium control in cells (a goal that is actively pursued in our laboratory), the technique was also found to provide a means to characterize photochemistry and physical chemistry of Ca^{2+} -reactive molecules.

The instrument was purchased with an S10 NCRR award and Hasterlik Family matching funds. Supported by Conicyt Uruguay, NIAMS, NHLBI, and MDA.

22. Combined Phosphoinositide and Ca^{2+} Signals Mediating Intracellular Receptor Specificity toward Neuronal

Ion Channels. OLEG ZAIKA and MARK S. SHAPIRO,
Department of Physiology, University of Texas Health Science Center at San Antonio, San Antonio, TX 78229

Phosphatidylinositol (PI) 4,5-bisphosphate (PIP₂) regulates a plethora of ion channels and transporters, including voltage-gated N- and P/Q-type Ca²⁺ (I_{Ca}) and M-type K⁺ currents in neurons. Of four G_{q/11}-coupled, PLC-linked receptors in superior cervical ganglion (SCG) sympathetic neurons, the M₁ muscarinic and AT₁ angiotensin II types do not elicit Ca²⁺_i signals and suppress both types of currents via depletion of PIP₂, whereas the B₂ bradykinin and P2Y purinergic types elicit robust IP₃-mediated [Ca²⁺]_i rises, do not deplete PIP₂ nor inhibit I_{Ca}, and suppress M current via Ca²⁺/calmodulin action. We have suggested that this receptor specificity toward the channels arises from differential Ca²⁺_i signals, underlying receptor-specific stimulation of PIP₂ synthesis by PI 4 kinase. Here, we inquire more deeply into these phenomena, asking which PI 4 kinase isoform underlies this signal, whether stimulation of PI(4) 5 kinase is also required to maintain PIP₂ levels during PLC activity, and the origin of receptor specificity in Ca²⁺_i signals. We used recordings of endogenous I_{Ca} as a “biosensor” of PIP₂ levels from SCG cells treated with pertussis toxin to isolate G_{q/11}-mediated signaling. In control neurons, stimulation of M₁ receptors with 10 μM oxotremorine methiodide (oxo-M) robustly suppressed I_{Ca}, but the application of 250 nM bradykinin or 10 μM of the P2Y agonist, uridine 5'-triphosphate (UTP) had little effect on I_{Ca}, reporting that only M₁ receptor stimulation depletes PIP₂ levels. However, when cells were pretreated with the specific PI 4 kinase IIIβ inhibitor PIK93 (0.3 μM; 7 min) or with DAG kinase inhibitor II (R59949; 20 μM, 1 h), all three agonists suppressed I_{Ca} to varying degrees, and the two drugs together did not have a greater effect. Because DAG kinase converts DAG into phosphatidic acid (PA), which is known to stimulate PI(4) 5 kinase, these data suggest that stimulation of PI 4 kinase IIIβ and PI(4) 5 kinase is required to prevent PIP₂ depletion by receptors. PI(4) 5 kinase is also thought to be stimulated by RhoA and its effector, Rho kinase. Indeed, when endogenous Rho activity was blocked by transfection of dominant-negative RhoA T19N, or when Rho kinase was blocked by pretreatment of cells with 1 μM Y27632 (40 min), UTP, BK, and oxo-M all suppressed I_{Ca} to varying degrees. Transfection of RhoA T19N also reduced tonic I_{Ca} amplitudes. Localization of certain G_{q/11}-coupled receptors with IP₃ receptors has been postulated to explain receptor-specific Ca²⁺_i signals. As a test, we compared agonist-induced [Ca²⁺]_i rises in neurons transfected with EGFP only or together with exogenous M₁ receptors. The former responded to UTP and BK, but not oxo-M, with robust Ca²⁺_i signals, whereas in the latter, the response to oxo-M was large, suggesting that microdomain organization plays a strong role. We also tested the part played by an

endogenous inhibitory protein of IP₃ receptors, IRBIT, which we found localizes to SCG neurons by immunostaining. Over-expression of wild-type IRBIT decreased the percentage of SCG cells responding to BK or UTP with Ca²⁺_i signals, but it only slightly affected the amplitude of the evoked [Ca²⁺]_i rises. Over-expression of dominant-negative IRBIT S68A had little effect on the responses to BK or UTP, but it greatly increased the percentage of cells responding to oxo-M with Ca²⁺_i signals. We conclude that overlaid on microdomain organization is IRBIT activity, which sets a “threshold” for [IP₃] for opening in the vicinity of the IP₃ receptor, assisting in the fidelity of receptor specificity in intracellular Ca²⁺ signaling, downstream agonist-specific depletion of PIP₂ and consequential receptor-specific depression of I_{Ca} and other PIP₂-sensitive conductances in neurons.

Supported by National Institutes of Health grants R01 NS43394 and ARRA-R01 NS065138 to M.S. Shapiro.

23. Protein Localization Using Correlative Super Resolution Fluorescence Microscopy and Electron Microscopy. SHIGEKI WATANABE,¹ ANNEDORE PUNGE,² GUNTHER HOLLOPETER,¹ ROBERT JOHN HOBSON,¹ M. WAYNE DAVIS,¹ STEFAN W. HELL,² and ERIK M. JORGENSEN,¹ ¹*Department of Biology and Howard Hughes Medical Institute, University of Utah, Salt Lake City, UT 84112;* ²*Department of NanoBiophotonics, Max Planck Institute for Biophysical Chemistry, 37077 Göttingen, Germany*

To fully understand the cell biology of synapses, the location of proteins relative to features such as the active zone and synaptic vesicles needs to be revealed. Immunofluorescence or genetically encoded fluorescent proteins have been used extensively to identify subcellular localization of proteins. However, the resolution of fluorescence microscopy is limited to around 200 nm by the diffraction of light (Born, M., and E. Wolf. 2002. *Principles of Optics*. Cambridge University Press, Cambridge)—a resolution that is not useful given the size of structures at synapses. Recently, several microscopy techniques, namely STED (Hell, S.W., and J. Wichmann. 1994. *Opt. Lett.* 19:780–782) and PALM (Betzig, E., G.H. Patterson, R. Sougrat, O.W. Lindwasser, S. Olenych, J.S. Bonifacino, M.W. Davidson, J. Lippincott-Schwartz, and H.F. Hess. 2006. *Science*. 313:1642–1645) or STORM (Rust, M.J., M. Bates, and X. Zhuang. 2006. *Nat. Methods* 3:793–795), have been developed to overcome this resolution limit. Proteins can be localized at 20-nm resolution. One drawback of fluorescence-based approaches is that the cellular context is often absent from the image. On the other hand, immuno-electron microscopy (immuno-EM) depicts subcellular structure, but protein localization in electron micrograph is limited by sample preparation and availability of antibodies (Roth, J., M. Bendayan, E. Carlemalm, W. Villiger, and M. Garavito. 1981. *J. Histochem. Cytochem.* 29:663–671).

Combining the super-resolution microscopy techniques with electron microscopy could merge the protein localization advantages of fluorescence microscopy with the structural information of electron microscopy. Thus, we have developed techniques to localize fluorescently tagged proteins in tissue samples that are compatible with electron microscopy. Fusion proteins tagged with Citrine or tdEos were preserved during specimen fixation and embedding. Fluorescence localizations revealed by STED or PALM were correlated with organelles imaged in electron micrographs from the same sections. This correlative method will be used to localize synaptic proteins within *Caenorhabditis elegans* synapses.

Sponsored by funding awarded to E.M. Jorgensen.

24. Label-free Cellular Imaging by Wide-Field Surface Plasmon Resonance Microscopy. KEVIN F. WEBB and NOAH A. RUSSELL, *Institute of Biophysics, Imaging and Optical Science, School of Electrical and Electronic Engineering, University of Nottingham, Nottingham NG7 2, England, UK*

Long-term observation of cell behavior is crucial to the investigation of many physiological processes. Exposure to transmitted incident light is directly detrimental to cell health and excites and bleaches fluorophores throughout the cell. Evanescent field methods such as TIRF use very high angles of illumination to produce total internal reflection at the coverslip interface. An evanescent field extends ~100 nm into the preparation, restricting excitation to within this restricted volume. Surface plasmon resonance (SPR) microscopy involves the incorporation of a 50-nm gold layer at the coverslip surface, upon which cells are cultured attached to an aminothiol self-assembled monolayer. By adjusting the angle of illumination at the back aperture of a high-NA objective lens, plasmon resonance is evoked whereby incident photons excite plasmons in the metal electrons and very little light is reflected. The resonant angle is very sensitive to the refractive properties of material within the evanescent field, providing high contrast in reflectance mode. The evanescent field is amplified at the surface by SPR, allowing TIRF-like studies at lower illumination intensities. An imaging system has been constructed incorporating a 1.49-NA objective for TIRF/TIRM/SPR, in addition to transmitted, reflectance, and epifluorescent imaging from above. High resolution in XY and very high contrast is achieved over a field of ~300 μ m. Primary neurons, cardiac myocytes, and fibroblast cell lines have been cultured on SPR surfaces and imaged over periods of hours. Dynamic cell events such as cytoplasmic extension, membrane process formation, and movement, etc., can be followed over long periods, with appropriate homeostasis being maintained. The sensitivity of SPR also allows surface layers, such as self-assembled monolayers, extracellular matrix, or cell adhesion deposits to be detected. Long-term, label-free live cell imaging by wide-field SPR micros-

copy thus offers a minimally invasive, highly flexible modality that may be of considerable use in cellular physiology.

25. Visualization of Repeated Synaptic Vesicle Recycling. BENJAMIN G. WILHELM^{1,2} and SILVIO O. RIZZOLI,¹

¹*European Neuroscience Institute, 37077 Göttingen, Germany;*

²*International Max Planck Research School Neuroscience, 37077 Göttingen, Germany*

Synaptic transmission at chemical synapses relies on the release of neurotransmitters via synaptic vesicle exocytosis. Two modes of release have been described: spontaneous (at rest) and active (during stimulation). It has been thought for decades that the vesicles releasing actively or spontaneously are identical, especially as they contain precisely identical levels of neurotransmitter. However, several recent studies on hippocampal cultured neurons suggested that the two release modes are supported by distinct synaptic vesicle populations. This notion is currently a highly contested one, and so far based exclusively on cultured synapses. To test this hypothesis, we investigated the release of FM 1-43 (which is directly proportional to the rates of exocytosis) in several preparations. Presynaptic vesicles were loaded with FM 1-43 by active or spontaneous exo-endocytosis, and were subsequently unloaded either actively or spontaneously. If different vesicles maintain active and spontaneous release, the FM dye loaded by one paradigm would only be released by the same paradigm. This was not the case in hippocampal neurons, and neither in three mature neuromuscular synapses (from mouse, frog, and *Drosophila*): vesicles were released equally well spontaneously or actively, regardless of the loading procedure. To further confirm the FM-derived results in hippocampal neurons, we used a novel assay in which recycling vesicles were labeled in a first round (either actively or spontaneously) with antibodies against the vesicle marker synaptotagmin, followed by secondary detection of the antibody in a following round (again, actively or spontaneously). All labeling combinations provided the same levels of fluorescence, again suggesting that the same vesicles can be released both spontaneously and actively. We therefore conclude that synaptic vesicles recycled at rest and during synaptic activity are identical. (Prof. Dr. Erwin Neher)

26. Mapping the Structure of CLC-1 Using Fluorescence Resonance Energy Transfer. YAWEI YU, XIAODONG ZHANG, WEI-PING YU, and TSUNG-YU CHEN, *Center for Neuroscience and Department of Neurology, University of California, Davis, Davis, CA 95618*

CLC-1, a member of the CLC channel/transporter family expressed on the cell membrane of skeletal muscles, contributes to >50% of the resting membrane conductance of the skeletal muscle. Although the crystal structure of bacterial CLC as well as the cytoplasmic

domain of various mammalian CLC molecules has been solved (Dutzler, R., E.B. Campbell, and R. MacKinnon. 2003. *Science*. 300:108–112; Meyer, S., and R. Dutzler. 2006. *Structure*. 14:299–307; Markovic, S., and R. Dutzler. 2007. *Structure*. 15:715–725; Meyer et al., 2007), the high-resolution structure of CLC-1 remains elusive. In this study, we use the fluorescence resonance energy transfer (FRET) technique to map the general structure of CLC-1 and study its structure–function relationship. We conducted FRET experiments by tagging CFP and YFP to different positions of CLC-1. By tagging N terminus and C terminus of CLC-1 with CFP and YFP simultaneously, a low FRET efficiency of merely ~5% was detected. However, with only about 100 amino acids truncated from the C terminus, the FRET efficiency dramatically increased to about 22%. Using this approach, we are able to compare the structure of CLC-1 with CLC-0 and other members of the CLC chloride channel/transporter family. The results suggest a structural architecture consistent with various high resolution structures from other CLC family members.

27. Two-Photon Imaging of Phototransduction Proteins in Living Mouse Rods. DELAINE LARSEN, NATHAN MELLING, MARIE BURNS, and EDWARD N. PUGH JR., *Center for Neuroscience, University of California, Davis, Davis, CA 95618*

Background. Arrestin1 (Arr1) is a 48-kD protein essential for the normal deactivation of photoactivated rhodopsin in rod photoreceptors during phototransduction, and is the second most abundant protein in rods after rhodopsin. In the dark-adapted rod, Arr1 is primarily excluded from the outer segment, where it interacts with rhodopsin; this has been shown using immunohistochemical techniques in several species, serial cryosectioning with Western blotting in mice and confocal imaging of an Arr1-eGFP fusion protein in *Xenopus*. After exposure to steady light, the subcellular distribution of Arr1 changes, with a dramatic translocation to the outer segment. Investigations of the physiological consequences of Arr1 translocation in living rods has been impeded by the fact that standard imaging techniques used to image Arr1 also induce its translocation. To overcome this impediment and lay the grounds for electrophysiological characterization of single rods with

measured quantities of Arr1 in the outer segment, we have used two-photon (2p) imaging of a tdTomato-Arr1 (tdTom-Arr1) fusion protein expressed in mouse rods to measure its translocation in living retinal slices under conditions amenable to electrophysiology.

Methods. TdTom-Arr1 fusion protein was expressed in c57B/6 mouse rods under the rhodopsin promoter using neonatal electroporation. Small retinal slices were dissected under infrared (IR) viewing and loaded into a flow chamber on the stage of an inverted microscope. Rapid rastering of the chamber viewfield using transmitted IR viewing allowed selection of properly oriented slices for 2p imaging. TdTom fluorescence was excited with a Ti-sapphire laser (Coherent Ultra II) tuned to 920 nm focused to its diffraction limit, and collected with photon-counting photodiodes, with 3-D scanning under control of a customized LabView interface (Calvert, P.D., W.E. Schiesser, and E.N. Pugh Jr. 2010. *J. Gen. Physiol.* 135:173–196). Laser exposure was kept to the minimum required to reliably observe tdTom fluorescence, as confirmed with emission spectra analysis.

Results. Overall expression of tdTom-Arr1 varied from cell to cell, but the normalized distribution of the protein was highly consistent. Calibration of tdTom fluorescence using purified recombinant proteins was made using the known extinction coefficients, and revealed the fusion protein to be at 50–300 μ M, ~1/60th to 1/10th the endogenous level of Arr1. The vast majority of tdTom-Arr1 was located in the inner segment and synaptic regions of dark-adapted rods. After a strong light exposure, most of the tdTom-Arr1 translocated from the inner segment to the outer segment over a time course of several minutes.

Conclusions. We have used 2p imaging to measure the translocation of an Arr1 fusion protein in living mouse retinal rods at high temporal and spatial resolution. The preliminary data show that the method sufficiently minimizes effective visible light exposure to capture sequential images of tdTom-Arr1 localization in its dark-adapted distribution. The ability to use 2p imaging to measure the concentration of Arr1 in outer segments without strongly driving phototransduction will be pivotal in future studies determining how Arr1 levels affect the gain and kinetics of the rod's electrical photoresponse.

INDEX TO AUTHORS OF ABSTRACTS

Abstract number follows name

Angueyra, J.M., 7
 Arant, R.J., 18
 Bamberg, E., 5
 Blatter, L., 21
 Bouchard, M.B., 1, 2, 10
 Brewka, R.R., 17
 Brum, G., 21
 Bunnell, S.C., 17
 Burns, M., 27
 Chen, B.R., 2
 Chen, T.-Y., 26
 Chen, Z., 3
 Clusin, W.T., 4
 Contreras, J., 6
 Cornish, V.W., 3, 13
 Curci, S., 11, 15
 Davis, M.W., 23
 DeGnore, J., 17
 del Pilar Gomez, M., 7, 8, 9
 Dempski, R.E., 5
 Elkabes, S., 14
 Ellis-Davies, G., 21
 Espinosa, L., 8
 Fakira, A.K., 14
 Figueroa, L., 21
 Foskett, J.K., 18
 Gallagher, S.S., 3, 13
 Gaspers, L.D., 14
 Geys, S., 5
 Giraldez, T., 6
 Gregg, J.L., 19
 Grosberg, L.E., 10
 Hagen, B., 16
 Hell, S.W., 16, 23
 Hillman, E.M.C., 1, 2, 10
 Hobson, R.J., 23
 Hofer, A.M., 11, 15, 18
 Hollopeter, G., 23
 Holmgren, M., 6
 Ianowski, J.P., 18
 Illek, B., 18
 Isacoff, E., 18
 Jacob, T.C., 12
 Jing, C., 13
 Jorgensen, E.M., 23
 Kohl, T., 16
 Larsen, D., 27
 Lauterbach, M.A., 16
 Lechleiter, J.D., 20
 Lederer, W.J., 16
 Lefkimiatis, K., 11, 15
 Lehnart, S.E., 16
 Leronni, D., 11
 L'heureux, B., 2
 Li, Y., 21
 Lovy-Wheeler, A., 17
 Machen, T.E., 18
 Maiellaro, I., 15, 18
 Malagón, G., 7
 Matthes, E., 18
 McCaslin, A.F.H., 2
 Melling, N., 27
 Michels, G., 12
 Miranda, P., 6
 Model, M.A., 19
 Momotake, A., 21
 Moss, S.J., 12
 Nasi, E., 7, 8, 9
 Pandya, S.M., 19
 Paredes, R.M., 20
 Pugh, E.N., 27
 Pulido, C., 7
 Punge, A., 23
 Radosevich, A.J., 10
 Ramirez, N., 8
 Ríos, E., 21
 Rizzoli, S.O., 25
 Russell, N.A., 24
 Shapiro, M.S., 22
 Sheetz, M.P., 3
 Shi, J., 18
 Shkryl, V., 21
 Sigworth, F., 6
 Sylvain, N.R., 17
 Thomas, A.P., 14
 Vais, H., 18
 Wagner, E., 16
 Watanabe, S., 23
 Webb, K.F., 24
 Wesch, D., 6
 Westphal, V., 16
 Wilhelm, B.G., 25
 Wong, S., 18
 Yi, J., 21
 Yu, W.-P., 26
 Yu, Y., 26
 Zaika, O., 22
 Zhang, X.-D., 26
 Zhou, J., 21